

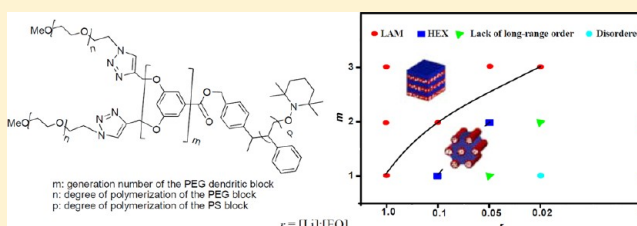
# Effects of Dendron Generation and Salt Concentration on Phase Structures of Dendritic–Linear Block Copolymers with a Semirigid Dendron Containing PEG Tails

Huanhuan Cai, Guoliang Jiang, Zhihao Shen,\* and Xinghe Fan\*

Beijing National Laboratory for Molecular Sciences, Key Laboratory of Polymer Chemistry and Physics of Ministry of Education, College of Chemistry and Molecular Engineering, Peking University, Beijing 100871, China

## Supporting Information

**ABSTRACT:** We prepared a series of dendritic–linear block copolymers (DLBCPs) bearing a semirigid Percec-type dendron with ionophilic poly(ethylene glycol) (PEG) tails and a polystyrene (PS) linear polymer by nitroxide-mediated living radical polymerization (NMRP). As the DLBCPs are connected by an ester linkage, through hydrolysis the molecular weights of the DLBCPs were precisely characterized by gel permeation chromatography and MALDI-TOF MS. Differential scanning calorimetry, small-angle X-ray scattering, and transmission electron microscopy were used to investigate the phase behaviors of the DLBCPs. Results show that the PEG tails of the semirigid dendron display a cold crystallization peak and a melting peak during the second heating process, while for the neat DLBCPs, the crystallization of the PEG tails is completely inhibited, and only the glass transition temperature ( $T_g$ ) of the PS block is observed. However,  $T_g$  of the dendron block can be observed by complexing the DLBCPs with  $\text{LiCF}_3\text{SO}_3$ , suggesting that microphase separation occurs in the doped DLBCPs. Comparing the phase behaviors of the DLBCPs having the same dendron weight fraction ( $w_D = 0.14$ ) with varying dendron generation and salt concentration, we found that the  $G_1$  or  $G_2$  DLBCP undergoes a phase transition from a hexagonally packed cylinder structure to a lamellar structure with increasing content of  $\text{LiCF}_3\text{SO}_3$ . However, the  $G_3$  DLBCP only displays a lamellar phase, and the lamellar thickness increases with increasing salt concentration. The difference can be attributed to the different degree of chain branching, which leads to different interface curvature.



## INTRODUCTION

Generally, block copolymers (BCPs) composed of two chemically different, covalently bonded polymers can self-assemble into various periodic nanostructures, such as lamella, cylinder, gyroid, and sphere.<sup>1</sup> The morphologies of the coil–coil diblock BCPs are determined by the volume fraction  $f$  of one block, the Flory–Huggins interaction parameter  $\chi$ , and the total degree of polymerization  $N$ . We can easily control the degree of polymerization and vary the composition of the BCPs chemically. Meanwhile, some methods have been used to change the interaction parameter  $\chi$  physically. For example, selective coordination of ion salts to the ionophilic block component such as poly(ethylene glycol) (PEG) derivatives influences the sizes of the microphases and transition behaviors in ion-doped BCPs which can be candidates as electrolytes in electrochemical devices.<sup>2</sup> In addition, ordered mesoporous materials with high electrical conductivity have been synthesized from coassembly of metal nanoparticles and block copolymers.<sup>3</sup>

Dendrimer has drawn considerable attention because of its precise molecular weight (MW), unique three-dimensional architecture, monodisperse character, and small hydrodynamic radius.<sup>4</sup> In addition, a large number of reactive groups at periphery of the dendrimer can be modified with functional

groups. Combining dendrimer with linear polymers produces dendritic–linear block copolymers (DLBCPs), which have been proposed in 1993.<sup>5</sup> Many previous publications devote to the study of bulk and solution properties.<sup>6–15</sup> Results have shown that the branched molecular architecture of DLBCPs largely shifts the phase boundary in comparison to linear BCPs.<sup>16</sup> Cho et al. have extensively investigated the self-assembly behavior of amphiphilic dendrons extended with linear crystallizable PEG chains and their ionic complexes by changing the dendron generation or the length of the linear block.<sup>17–21</sup> The phase structures are closely related to crystallization of the PEG segments. The phase behavior of DLBCPs consisting of a third-generation coil dendron modified with low molecular weight PEG and a coil linear block polystyrene (PS) was also explored, and the morphology changes from lamella (LAM) to a hexagonally packed cylinder (HEX) structure as the salt content increases.

We designed a series of DLBCPs (PEG( $G_m$ )-*b*-PS, where  $m$  is the generation number), in which the periphery of the semirigid Percec-type dendron blocks was used to introduce

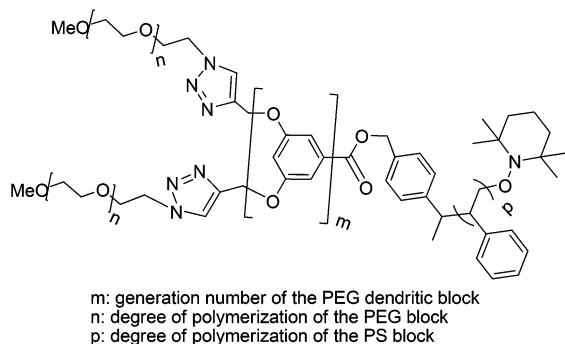
Received: March 30, 2012

Revised: July 11, 2012

Published: July 23, 2012

different number of ionophilic PEG chains, while the linear PS block and the semirigid dendron were used to maintain membrane toughness. The DLBCPs may have applications as conducting membranes, and chemical structures of the DLBCPs are shown in Chart 1.

Chart 1. Chemical Structures of DLBCPs



We studied the phase transition behaviors of ion-doped DLBCPs by exploring the influence of salt content and dendron generation on the bulk phase behaviors of the DLBCPs with the same dendron volume fraction. Our results show that the morphologies transform from disordered to hexagonally packed cylinders or lamellae as the salt content increases, which can be

attributed to an increase in  $\chi$  between the two block components because of the selective coordination of  $\text{LiCF}_3\text{SO}_3$  to the ionophilic PEG component.

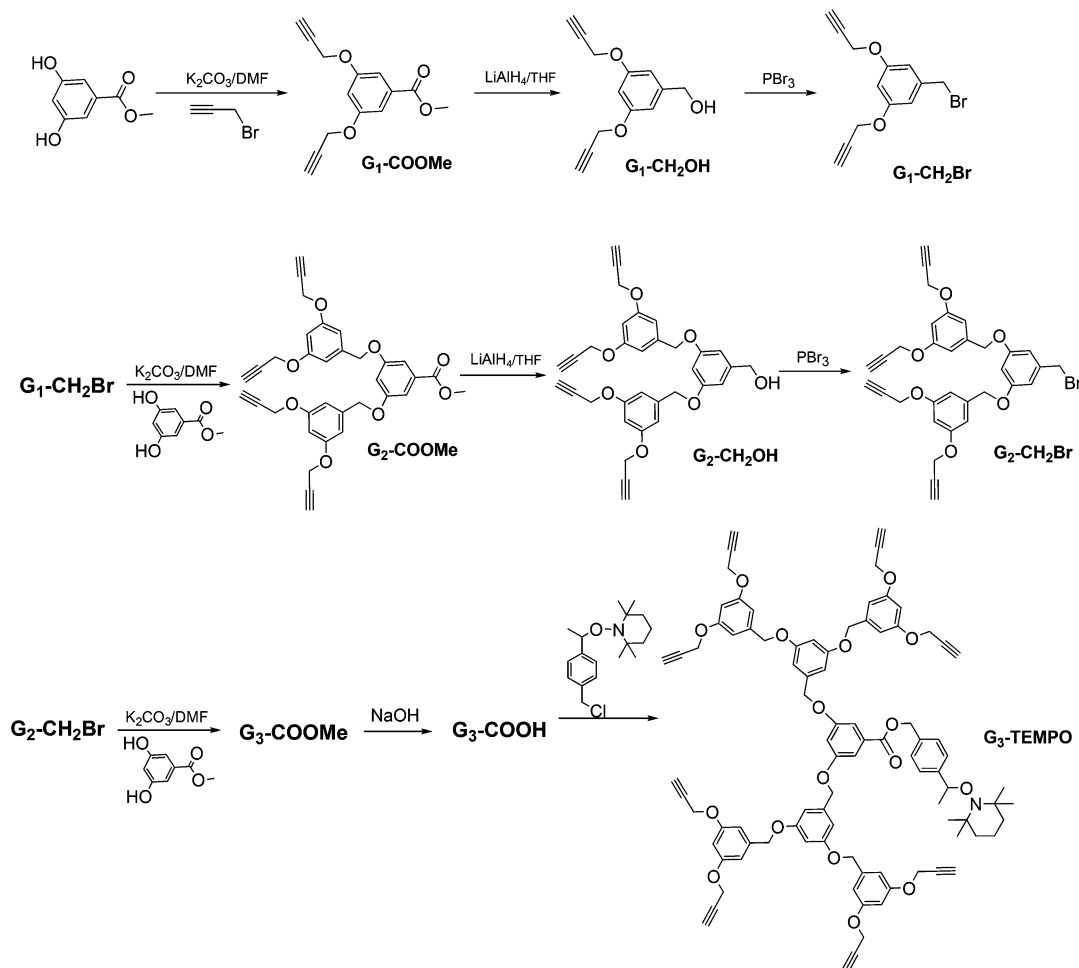
## EXPERIMENTAL SECTION

**Materials.** Traditional Percec-type benzyl ether dendrons were synthesized as described in the literature.<sup>22</sup> Triethylamine ( $\text{Et}_3\text{N}$ ), tetrahydrofuran (THF), and *N,N*-dimethylformamide (DMF) were distilled before use.  $\text{CuBr}$  was synthesized from  $\text{CuSO}_4$ ,  $\text{NaBr}$ , and  $\text{Na}_2\text{SO}_3$ , purified by washing with acetic acid, followed by washing with methanol, and then dried under vacuum. PEG with a molecular weight of 750 g/mol and lithium trifluoromethanesulfonate ( $\text{LiCF}_3\text{SO}_3$ ), both obtained from Aldrich, were dried under vacuum overnight. All other reagents were used as received from commercial sources.

**$\text{LiCF}_3\text{SO}_3$  Doping.** A measured amount of DLBCPs was dissolved in dry THF, followed by the addition of the appropriate amount of the salt. The mixture was stirred for 24 h. Then the solvent was removed under vacuum at 30 °C. The molar ratio of  $\text{LiCF}_3\text{SO}_3$  to PEG( $G_m$ )-*b*-PS, denoted as  $r = [\text{Li}]/[\text{EO}]$ , was varied from 0 to 1.

**Characterization.**  $^1\text{H}$  NMR spectra were recorded on a Bruker 300 or 400 MHz spectrometer.  $^{13}\text{C}$  NMR spectra were recorded on a Bruker 400 or 500 MHz spectrometer. Elemental analysis (EA) was carried out with an Elementar Vario EL instrument. Matrix-assisted laser desorption ionization time-of-flight mass spectrometry (MALDI-TOF MS) measurements were performed on a Bruker Autoflex high-resolution tandem mass spectrometer. Gel permeation chromatography (GPC) measurements were performed on a Waters 2410 instrument equipped with a Waters 2410 RI detector and three Waters  $\mu$ -Styragel columns ( $10^3$ ,  $10^4$ , and  $10^5$  Å), using THF as the eluent at a

Scheme 1. Synthetic Routes of  $G_m$ -X



flow rate of 1.0 mL/min at 35 °C. All GPC data were calibrated with linear polystyrene standards. Thermogravimetric analysis (TGA) was performed on a TA SDT 2960 instrument at a heating rate of 20 °C/min in a nitrogen atmosphere. Differential scanning calorimetry (DSC) examination was carried out on a TA DSC Q100 calorimeter with a programmed heating procedure in nitrogen. The sample had a size of 2–5 mg and sealed in an aluminum pan. The temperature and heat flow scale at different cooling and heating rates were calibrated using standard materials such as indium. Glass transition temperatures ( $T_g$ 's) were obtained from the second heating scans.

Small-angle X-ray scattering (SAXS) experiments were conducted on a Bruker NanoStar U SAXS system using a Cu  $K\alpha$  radiation source ( $\lambda = 0.154$  nm at 40 kV and 35 mA). SAXS samples were sealed in aluminum foil while acquiring scattering data under vacuum. One-dimensional SAXS data are presented as  $Iq^2$  vs  $q$ , where  $q$  is the azimuthally integrated intensity and  $q$  is scattering vector ( $q = 4\pi \sin \theta / \lambda$ , where  $2\theta$  is the scattering angle).

Transmission electron microscopy (TEM) micrographs were obtained on a JEM-2100 electron microscope at an acceleration voltage of 200 kV. The solution-cast sample films were stained with RuO<sub>4</sub> vapor for 3 min to enhance contrast. RuO<sub>4</sub> reacted with both blocks of the copolymer, and the PEG part was stained first.

The ionic conductivity of the polymer electrolyte film was measured using a cell which was assembled by sandwiching the film between two stainless steel disk electrodes. The polymer electrolyte film was prepared by solution-casting in humid atmosphere before dried under vacuum at 100 °C. The ionic conductivity ( $\sigma$ ) values were determined by electrical impedance spectrum measurements (EIS, EG&G potentiostat/galvanostat model 283), and the samples were thermally equilibrated at each temperature for 0.5 h before measurement. The conductivity values can be calculated from the relationship  $\sigma = l / (R_b A)$ , where  $R_b$  is the bulk electrolyte resistance,  $l$  is the thickness, and  $A$  is the area of the film.

**Synthesis of Acetylene-Terminated Dendrons.** The synthetic routes of the dendron intermediates ( $G_m-X$ , where  $m$  denotes the generation number and  $X$  is the functional group at the focal point) are depicted in Scheme 1. The experimental details are described below using  $G_1-X$  as an example. Other <sup>1</sup>H NMR data of dendron intermediates are provided in the Supporting Information.

**General Procedure for Alkylation.**  $G_1-COOME$ . Potassium carbonate (15.1 g, 109 mmol) and 18-crown-6 (0.1 g, 0.4 mmol) were added to a stirred solution of propargyl bromide (29.7 g, 220 mmol) and methyl 3,5-dihydroxybenzoate (16.8 g, 100 mmol) in acetone (300 mL). The reaction mixture was heated to reflux under nitrogen for 24 h, filtered, evaporated to dryness, and partitioned between water and CH<sub>2</sub>Cl<sub>2</sub>. The aqueous layer was then extracted with dichloromethane (200 mL), and the combined extracts were dried over Na<sub>2</sub>SO<sub>4</sub>, evaporated, and washed with methanol to give the product as pale yellow crystals. Yield: 63%. <sup>1</sup>H NMR (300 MHz, CDCl<sub>3</sub>,  $\delta$ , ppm): 2.54 (t,  $J = 2.4$  Hz, 2H, C $\equiv$ CH), 3.91 (s, 3H, CH<sub>3</sub>O), 4.72 (d,  $J = 2.4$  Hz, 4H, CH<sub>2</sub>C $\equiv$ CH), 6.82 (s, 1H, *p*-Ar), 7.30 (d,  $J = 2.4$  Hz, 2H, *o*-Ar).

**General Procedure for Reduction.**  $G_1-CH_2OH$ . Lithium aluminum hydride (3.99 g, 105 mmol) was added to a stirred solution of the ester  $G_1-COOME$  (20.6 g, 84.4 mmol) in anhydrous THF (500 mL) in small portions, and the reaction mixture was stirred at ambient temperature for 2 h. Water was then added slowly to stop the reaction. The reaction mixture was filtered under vacuum, the solid rinsed with CH<sub>2</sub>Cl<sub>2</sub>, and the filtrate dried with MgSO<sub>4</sub>. After evaporation of the solvents, the alcohol was purified by recrystallization from methanol and recovered as white crystals. Yield: 90%. <sup>1</sup>H NMR (300 MHz, CDCl<sub>3</sub>,  $\delta$ , ppm): 2.53 (t,  $J = 2.4$  Hz, 2H, C $\equiv$ CH), 4.65 (s, 2H, CH<sub>2</sub>OH), 4.67 (d,  $J = 2.4$  Hz, 4H, CH<sub>2</sub>C $\equiv$ CH), 6.54 (s, 1H, *p*-Ar), 6.63 (d,  $J = 2.1$  Hz, 2H, *o*-Ar).

**General Procedure for Bromination.**  $G_1-Br$ . The synthetic procedure was similar to that reported in literature.<sup>23</sup> Phosphorus tribromide (27.1 mL, 280 mmol) was added dropwise to a stirred solution of the alcohol  $G_1-CH_2OH$  (20.56 g, 95 mmol) in anhydrous CH<sub>2</sub>Cl<sub>2</sub> (150 mL) at 0 °C under argon. Stirring was continued at 0 °C for 30 min and then at ambient temperature for 2 h. The reaction

mixture was poured into ice/water (400 mL) and extracted with CH<sub>2</sub>Cl<sub>2</sub>. The organic layer was separated, washed with brine (500 mL), dried over anhydrous Na<sub>2</sub>SO<sub>4</sub>, and evaporated to give the crude product, which was purified by silica gel column chromatography using petroleum ether/CH<sub>2</sub>Cl<sub>2</sub> (1:1, v/v) as the eluent to afford 23.6 g of  $G_1-Br$  as a white powder. Yield: 89%. <sup>1</sup>H NMR (300 MHz, CDCl<sub>3</sub>,  $\delta$ , ppm): 2.54 (t,  $J = 2.4$  Hz, 2H, C $\equiv$ CH), 4.67 (s, 2H, CH<sub>2</sub>Br), 4.69 (d,  $J = 2.4$  Hz, 4H, CH<sub>2</sub>C $\equiv$ H), 6.55 (s, 1H, *p*-Ar), 6.65 (d,  $J = 2.4$  Hz, 2H, *o*-Ar).

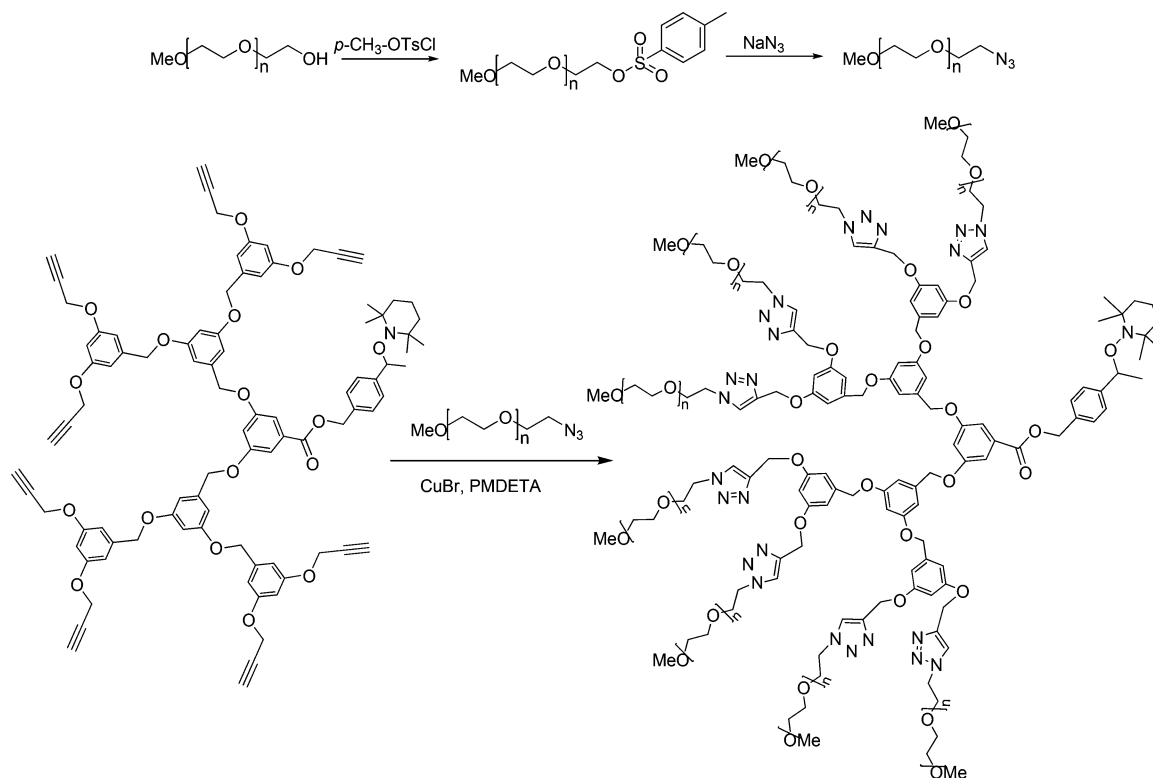
**General Procedure for Hydrolysis.**  $G_1-COOH$ . A procedure similar to that reported in literature<sup>24</sup> was employed.  $G_1-COOME$  was dissolved in a mixture of 60 mL of THF, 10 mL of CH<sub>3</sub>OH, and 10 mL of distilled water. Addition of sodium hydroxide was followed by stirring at 65 °C for 18 h. The pH of the mixture was adjusted to 3 using dilute aqueous HCl. The aqueous layer was separated and extracted with CH<sub>2</sub>Cl<sub>2</sub>, washed with brine three times, and dried over Na<sub>2</sub>SO<sub>4</sub>, and the solvent was removed to give the product as a pale yellow powder. Yield: 100%. <sup>1</sup>H NMR (400 MHz, DMSO,  $\delta$ , ppm): 3.61 (t,  $J = 1.2$  Hz, 2H, C $\equiv$ CH), 4.85 (d,  $J = 1.2$  Hz, 4H, CH<sub>2</sub>C $\equiv$ H), 6.85 (s, 1H, *p*-Ar), 7.16 (d,  $J = 1.2$  Hz, 2H, *o*-Ar). <sup>13</sup>C NMR (100 MHz, DMSO,  $\delta$ , ppm): 55.81 (2C), 78.61 (2C), 78.90 (2C), 106.97 (1C), 108.40 (2C), 132.91 (1C), 158.22 (2C), 166.77 (1C).

**Synthesis of 1-(4'-Chloromethylphenyl)-1-(2'',2'',6'',6''-tetramethyl-1-piperidinyloxy)ethyl (TEMPO-Cl).** The synthesis of TEMPO-Cl was carried out according to the method reported in the literature.<sup>25</sup> TEMPO (1.25 g, 8 mmol) and 4-vinylbenzyl chloride (1.8 g, 11.8 mmol) were dissolved in 10 mL of isopropyl alcohol in an open flask. The solution was vigorously stirred, and Mn(salen)Cl catalyst (357 mg, 1 mmol) was added, followed by the addition of NaBH<sub>4</sub> (492 mg, 13 mmol) in small portions for many times. After 24 h, the reaction was carefully quenched at 0 °C by addition of distilled water, and then the reaction mixture was partitioned between chloroform and distilled water. The organic layer was then dried and evaporated to dryness, and the crude product was purified by silica gel column chromatography using petroleum ether/CH<sub>2</sub>Cl<sub>2</sub> (6:1, v/v) as the eluent to afford the product (TEMPO-Cl) as a white crystal. Yield: 41.2%. <sup>1</sup>H NMR (300 MHz, CDCl<sub>3</sub>,  $\delta$ , ppm): 0.66, 1.02, 1.16, 1.28 (s, 12H, CH<sub>3</sub>), 1.25–1.54 (m, 6H, CH<sub>2</sub>), 1.45 (d,  $J = 6.9$  Hz, 3H, CH<sub>3</sub>), 4.59 (s, 2H, CH<sub>2</sub>Cl), 4.80 (q,  $J = 6.6$  Hz, 1H, CH), 7.26–7.34 (m, 4H, Ar).

**General Procedure for Esterification.**  $G_1-TEMPO$ . The synthesis was similar to the method reported in the literature.<sup>26</sup> Tetrabutylammonium fluoride (TBAF) was added to a solution of  $G_1-COOH$  (1.1 mmol) and TEMPO-Cl (1 mmol) in dry DMF. The mixture was stirred at 25 °C under N<sub>2</sub> for 24 h, and it was then poured into distilled water and extracted with CH<sub>2</sub>Cl<sub>2</sub>. The organic layer was separated, washed with brine (500 mL), dried over anhydrous Na<sub>2</sub>SO<sub>4</sub>, and evaporated to give the crude product, which was purified by silica gel column chromatography using CH<sub>2</sub>Cl<sub>2</sub> as the eluent to afford a white powder. Yield: 89%. <sup>1</sup>H NMR (400 MHz, CDCl<sub>3</sub>,  $\delta$ , ppm): 0.66, 1.02, 1.16, 1.28 (s, 12H, CH<sub>3</sub>), 1.25–1.54 (m, 6H, CH<sub>2</sub>), 1.45 (d,  $J = 8.8$  Hz, 3H, CH<sub>3</sub>), 2.54 (t,  $J = 3.2$  Hz, 2H, C $\equiv$ CH), 4.70 (d,  $J = 3.2$  Hz, 4H, CH<sub>2</sub>C $\equiv$ CH), 4.81 (q,  $J = 8.8$  Hz, 1H, CH), 6.80 (s, 1H, *p*-Ar), 7.34–7.39 (m, 6H, ArH). <sup>13</sup>C NMR (125 MHz, CDCl<sub>3</sub>,  $\delta$ , ppm): 17.32 (1C), 20.47 (1C), 23.72 (4C), 40.45 (2C), 56.26 (2C), 59.81 (2C), 66.98 (1C), 76.11 (2C), 78.05 (2C), 82.87 (1C), 107.48 (1C), 109.24 (2C), 126.85 (2C), 127.99 (2C), 132.38 (1C), 134.32 (1C), 146.10 (2C), 158.62 (2C), 165.92 (1C). Anal. Calcd for C<sub>31</sub>H<sub>37</sub>NO<sub>5</sub>: C 73.93, H 7.41, N 2.78. Found: C 73.88, H 7.38, N 2.82. HRMS:  $m/z$  504.273 89.

$G_2-TEMPO$ . This compound was prepared similarly according to the procedure for the synthesis of  $G_1-TEMPO$ . <sup>1</sup>H NMR (400 MHz, CDCl<sub>3</sub>,  $\delta$ , ppm): 0.66, 1.02, 1.16, 1.28 (s, 12H, CH<sub>3</sub>), 1.25–1.54 (m, 6H, CH<sub>2</sub>), 1.45 (d,  $J = 6.4$  Hz, 3H, CH<sub>3</sub>), 2.53 (t,  $J = 1.6$  Hz, 4H, C $\equiv$ CH), 4.68 (d,  $J = 1.6$  Hz, 8H, CH<sub>2</sub>C $\equiv$ CH), 4.80 (q,  $J = 6.8$  Hz, 1H, CH), 5.03 (s, 4H, ArCH<sub>2</sub>O), 6.58–7.39 (m, 13H, Ar). <sup>13</sup>C NMR (100 MHz, CDCl<sub>3</sub>,  $\delta$ , ppm): 17.34 (1C), 20.51 (1C), 23.74 (4C), 40.47 (2C), 56.09 (4C), 59.83 (2C), 66.96 (1C), 70.11 (2C), 75.94 (4C), 78.37 (4C), 82.86 (1C), 102.05 (2C), 107.01 (1C), 107.34 (4C), 108.83 (2C), 126.90 (2C), 128.04 (2C), 132.30 (1C), 134.37 (1C),

Scheme 2. Synthetic Routes of Dendritic Macroinitiators



139.12 (1C), 146.10 (2C), 159.01 (2C), 159.69 (4C), 166.18 (1C). Anal. Calcd for  $C_{51}H_{53}NO_9$ : C 74.34, H 6.48, N 1.70. Found: C 73.93, H 6.62, N 1.66. HRMS:  $m/z$  824.381 14.

**$G_3$ -TEMPO.** This compound was prepared similarly according to the procedure for the synthesis of  $G_1$ -TEMPO.  $^1H$  NMR (400 MHz,  $CDCl_3$ ,  $\delta$ , ppm): 0.68, 1.02, 1.15, 1.45, 1.47 (s, 21H,  $CH_3$ ), 2.51 (t, 8H,  $C\equiv CH$ ), 4.66 (d,  $J = 1.6$  Hz, 16H,  $CH_2C\equiv CH$ ), 4.79 (q,  $J = 6.8$  Hz, 1H, CH), 4.99 (2s, 12H,  $ArCH_2O$ ), 6.56–7.39 (m, 25H, Ar).  $^{13}C$  NMR (100 MHz,  $CDCl_3$ ,  $\delta$ , ppm): 17.33 (1C), 20.50 (1C), 23.74 (4C), 40.46 (2C), 56.07 (8C), 59.82 (2C), 66.97 (1C), 69.93 (6C), 75.92 (8C), 78.43 (8C), 82.86 (1C), 101.93 (6C), 106.67 (1C), 106.93 (12C), 108.72 (2C), 126.89 (2C), 128.07 (2C), 132.29 (1C), 134.39 (1C), 138.98 (1C), 146.09 (6C), 158.97 (6C), 159.76 (8C), 166.21 (1C). Anal. Calcd for  $C_{91}H_{83}NO_{17}$ : C 74.62, H 5.85, N 0.96. Found: C 74.56, H 5.95, N 1.02. HRMS:  $m/z$  1464.591 12.

**Synthesis of Dendritic Macroinitiators.** The synthetic routes are outlined in Scheme 2, with PEG( $G_3$ )-TEMPO as an example.

**Preparation of Azide-Terminated PEG (PEG- $N_3$ ).** The synthesis was performed according to the method reported in the literature.<sup>27</sup> Both poly(ethylene glycol) methyl ether ( $M_n = 750$  g/mol; 20.4 g, 27 mmol) and triethylamine (9.64 mL, 66 mmol) were completely dissolved in  $CH_2Cl_2$  (500 mL) under a  $N_2$  atmosphere. Toluene-4-sulfonyl chloride (7.9 g, 40 mmol) was added dropwise to the above solution in an ice/water bath, and then the resulting solution was stirred at ambient temperature for 24 h. Then the mixture was filtered under vacuum, and the liquid was dissolved in  $CH_2Cl_2$ , washed with brine (500 mL) three times, dried over anhydrous  $Na_2SO_4$ , and evaporated to give the monotosylated PEG. Yield: 95%.  $^1H$  NMR of PEG-Ts (300 MHz,  $CDCl_3$ ,  $\delta$ , ppm): 2.45 (s, 3H,  $ArCH_3$ ), 3.38 (s, 3H,  $CH_3O$ ), 3.46 (t,  $J = 3.3$  Hz, 2H,  $CH_3OCH_2$ ), 3.58 (t,  $J = 4.8$  Hz, 2H,  $CH_3OCH_2CH_2$ ), 3.64 (s, 450H,  $CH_2CH_2$ ), 3.82 (t,  $J = 4.8$  Hz, 2H,  $CH_2CH_2OTs$ ), 4.16 (t,  $J = 4.8$  Hz, 2H,  $CH_2CH_2OTs$ ), 7.36 (d,  $J = 8.1$  Hz, 2H, *o*-Ar), 7.81 (d,  $J = 8.4$  Hz, 2H, *p*-Ar). Subsequently, sodium azide (298.0 mg, 4.58 mmol) was added to a solution of the obtained PEG monotosylate (406.0 mg, 0.46 mmol) in dry DMF (10 mL) under a  $N_2$  atmosphere, and the reaction mixture was stirred vigorously at ambient temperature for 24 h. The product was dissolved in 80 mL of  $CH_2Cl_2$ . The mixture was extracted sequentially

with brine (100 mL) and distilled water and dried with anhydrous  $Na_2SO_4$ , and then the solvents were evaporated to yield PEG- $N_3$ . Yield: 90%.  $^1H$  NMR of PEO- $N_3$  (300 MHz,  $CDCl_3$ ,  $\delta$ , ppm): 3.38 (s, 3H,  $CH_3O$ ), 3.46 (t,  $J = 3.3$  Hz, 2H,  $CH_3OCH_2$ ), 3.54 (t,  $J = 4.8$  Hz, 2H,  $CH_2CH_2N_3$ ), 3.66 (s, 450H,  $CH_2CH_2$ ), 3.82 (t,  $J = 4.5$  Hz, 2H,  $CH_2CH_2N_3$ ).

**Preparation of Dendritic Macroinitiators.** The azide-terminated PEG, the dendritic initiator precursor, CuBr, and  $N,N,N',N''$ -pentamethyldiethylenetriamine (PMDETA) were added to a polymerization tube with dry DMF as solvent. After three freeze–pump–thaw cycles, the tube was sealed off under vacuum. Then the resulting solution was stirred at ambient temperature for 24 h. The tube was opened, and the reaction mixture was diluted with THF. CuBr was removed through a short neutral alumina column. DMF solvent was removed under a reduced pressure, and then the product was dissolved in 80 mL of  $CH_2Cl_2$ . The mixture was extracted sequentially with brine and distilled water, dried with anhydrous  $Na_2SO_4$ , and evaporated to yield the dendritic macroinitiator PEG( $G_3$ )-TEMPO.

**Synthesis of Block Copolymers.** All DLBCPs (PEG( $G_m$ )-*b*-PS) were obtained by bulk polymerization. For example, 2.62 g (25 mmol) of styrene and 0.21 g (0.03 mmol) of PEG( $G_3$ )-TEMPO were placed in a polymerization tube with a magnetic stir bar. After three freeze–pump–thaw cycles, the tube was sealed off under vacuum. Polymerization was carried out at 125 °C for 36 h. The tube was then opened, and the reaction mixture was diluted with THF. The resultant polymer was precipitated and washed with methanol. To eliminate the unreacted monomers and residual dendritic macroinitiator, the precipitate was redissolved in THF and then reprecipitated and washed with methanol until there were no peaks corresponding to the monomer and the initiator in the GPC profiles. After purification, the polymer was dried to a constant weight. Yield: 45%. The molecular weight of PEG( $G_3$ )-*b*-PS DLBCP is  $3.41 \times 10^4$  g/mol. By controlling the molar ratio of the dendritic macroinitiator to the styrene monomer, DLBCPs of varying dendron volume fractions were synthesized.

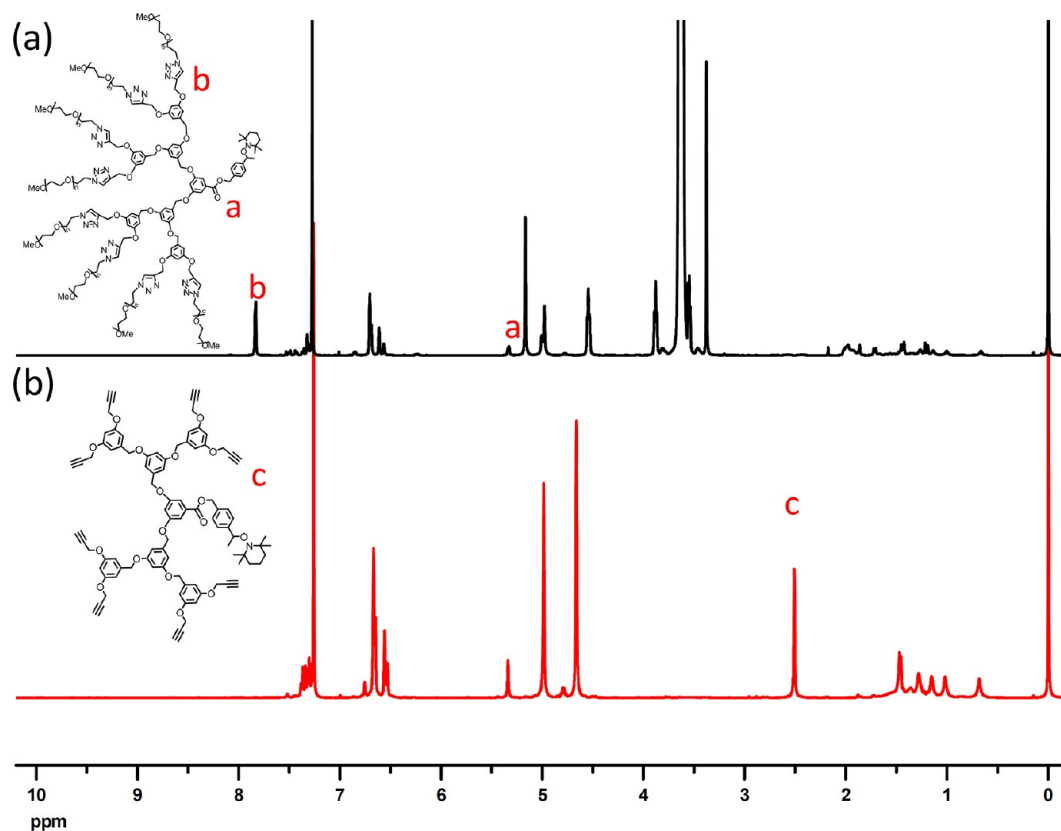


Figure 1.  $^1\text{H}$  NMR spectra of PEG( $G_3$ )-TEMPO (a) and  $G_3$ -TEMPO (b) in  $\text{CDCl}_3$ .

Table 1. Molecular Characteristics of All the Polymers

| sample                     | $M_n$ ( $\times 10^4$ g/mol) <sup>a</sup> | PDI  | $T_d$ ( $^\circ\text{C}$ ) <sup>b</sup> | $T_g$ ( $^\circ\text{C}$ ) <sup>c</sup> | $w_D$ <sup>d</sup> | $w_{\text{PEG}}$ <sup>e</sup> | $M_{n,\text{PS}}$ ( $\times 10^4$ g/mol) <sup>a</sup> | PDI <sub>PS</sub> |
|----------------------------|---|------|---|---|--------------------|-------------------------------|---|-------------------|
| PEG( $G_1$ )- <i>b</i> -PS | 1.30                                      | 1.09 | 328                                     | 75.4                                    | 0.14               | 0.11                          | 1.17  | 1.09              |
| PEG( $G_2$ )- <i>b</i> -PS | 2.07                                      | 1.18 | 353                                     | 95.8                                    | 0.18               | 0.13                          | 1.83  | 1.18              |
| PEG( $G_3$ )- <i>b</i> -PS | 3.41                                      | 1.23 | 334                                     | 98.4                                    | 0.16               | 0.13                          | 3.89  | 1.18              |

<sup>a</sup>The apparent number-average molecular weight ( $M_n$ ) and polydispersity index (PDI) were measured by GPC using PS standards. <sup>b</sup>The temperatures at 5% weight loss of the samples under nitrogen ( $T_d$ 's) were measured by TGA heating experiments at a rate of  $20^\circ\text{C}/\text{min}$ . <sup>c</sup>Evaluated by DSC during the second heating cycle at a rate of  $20^\circ\text{C}/\text{min}$ . <sup>d</sup>Mass fraction of the dendritic block. <sup>e</sup>Mass fraction of PEG.

## RESULTS AND DISCUSSION

**Synthesis and Characterization of Dendritic Macroinitiators and Polymers.** With PEG( $G_3$ )-TEMPO as an example, the dendritic macroinitiators were prepared with the synthesis of the acetylene-terminated dendrons, followed by esterification reaction to introduce TEMPO group at the focal point and the Huisgen's 1,3-dipolar cycloaddition reaction to modify the periphery of dendron with ionophilic PEG.<sup>28</sup> The structures of the precursors of the dendritic macroinitiators were confirmed by  $^1\text{H}$  NMR, MS, and EA. The disappearance of the resonance signals of the triplet with  $\delta = 2.51$  ppm arising from the proton of the terminal alkyne moiety verifies the completion of the coupling reaction, and a new peak at 7.78 ppm corresponding to the triazole ring is observed. Meanwhile, the ratio of the area of the triazole proton signals to that of the benzyl group signals in  $^1\text{H}$  NMR is calculated to be 4:1 (Figure 1).

DLBCPs were prepared through NMRP at  $125^\circ\text{C}$  for 24 h. Their compositions were determined by GPC and MALDI-TOF MS. As the two blocks are connected through an ester group, the DLBCPs can hydrolyze into two blocks. Molecular weights of the dendritic macroinitiators were measured by GPC

(Figure S4) and MALDI-TOF MS (Figure S5). Meanwhile, the molecular weight of the linear PS block can be precisely determined through GPC as all GPC data are calibrated with polystyrene standards (Figure S6). The PEG weight fractions and the thermal stability data of the DLBCPs are listed in Table 1. The weight fractions of the dendrons in the DLBCPs are all about 0.14–0.18.

DSC was used to investigate the thermal transitions of the dendritic macroinitiators and the neat and doped DLBCPs, with the results of PEG( $G_3$ )-*b*-PS shown in Figure 2 as an example. All other results are shown in the Supporting Information and are summarized in Table 1. DSC scans (Figure 2a) of the second heating process at a rate of  $20^\circ\text{C}/\text{min}$  show that the dendritic macroinitiator displays a glass transition at  $-49.8^\circ\text{C}$ , a cold crystallization peak at  $-15.6^\circ\text{C}$ , and a melting peak at  $27.0^\circ\text{C}$ . With the consideration of the composition of the dendritic macroinitiator, these peaks correspond to transitions of the PEG tail. For the neat DLBCP, the crystallization peak of PEG disappears completely, and only a glass transition at  $98.4^\circ\text{C}$  of the PS block is observed. With the lithium salt added, two distinct transitions at  $-28.6$  and  $99.3^\circ\text{C}$  are observed, corresponding to the glass

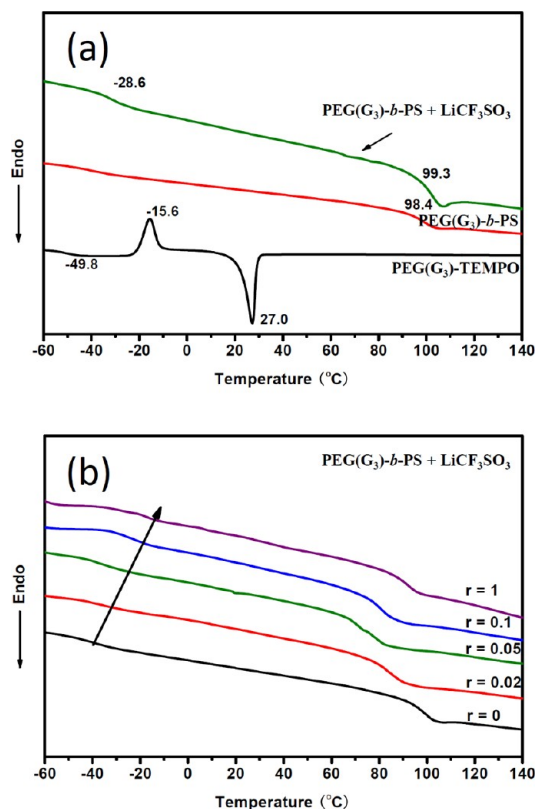


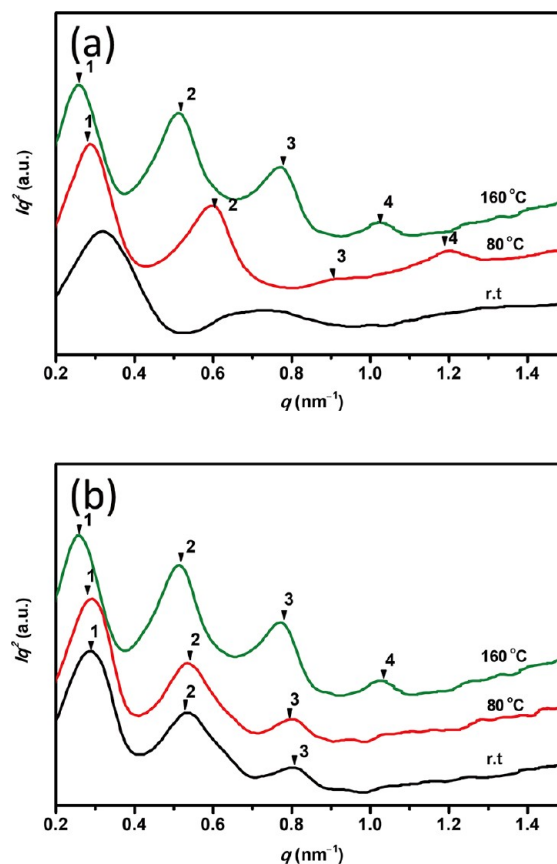
**Figure 2.** DSC second-heating thermograms of the dendritic macroinitiator PEG( $G_3$ )-TEMPO and the DLBCP without and with doped LiCF<sub>3</sub>SO<sub>3</sub> ( $r = 0.05$ ) (a) and those of the DLBCPs with different concentrations of the lithium salt (b).

transitions of the doped PEG peripheries and the linear PS block, respectively. The appearance of  $T_g$  of the dendritic block suggests that adding the lithium salt causes the DLBCPs to microphase separate. Meanwhile,  $T_g$  increases with increasing salt concentration (Figure 2b). This is attributed to increased ion-dipole interaction between Li<sup>+</sup> and the ether oxygens which results in decreased segmental mobility and stiffening of the chain. A similar phenomenon was observed for polyether-siloxane hybrids doped with LiClO<sub>4</sub>.<sup>29</sup>

#### Effect of Salt Concentration on Polymer Morphology.

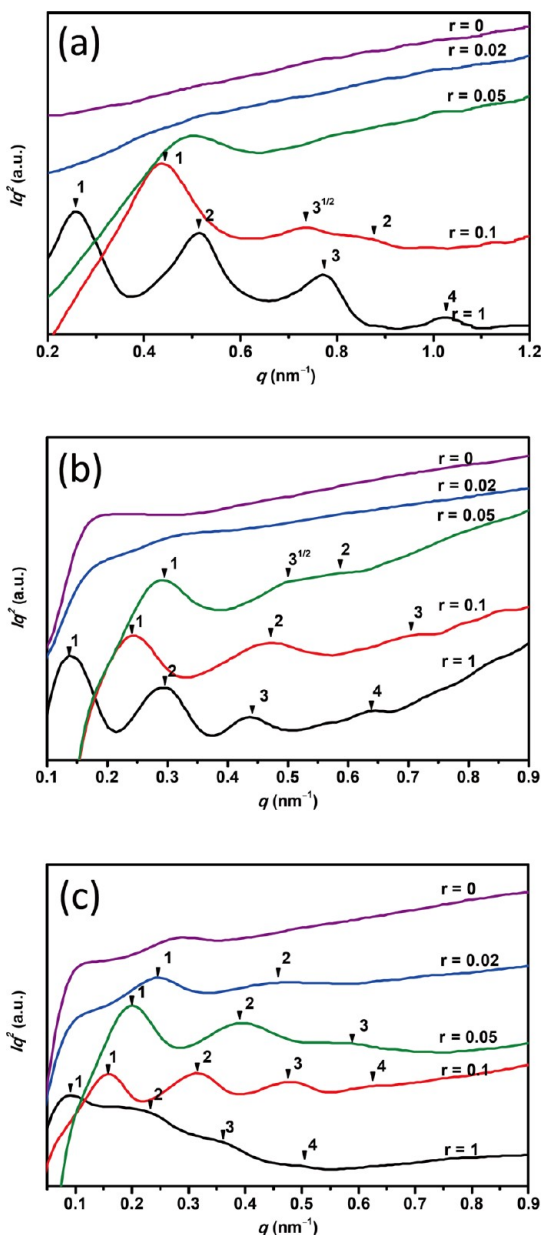
Variable-temperature SAXS experiments were performed up to 160 °C, well above the glass transition temperatures of PS and the dendron, to investigate the morphologies of the samples. The molar ratio of LiCF<sub>3</sub>SO<sub>3</sub> to EO in PEG( $G_m$ )-*b*-PS was varied to observe the effect of lithium salt concentration on phase behavior. The lithium concentration per ethylene oxide ([Li]/[EO]) was chosen to be 0, 0.02, 0.05, 0.1, and 1. Figure 3 shows the SAXS patterns of the LiCF<sub>3</sub>SO<sub>3</sub>-doped PEG( $G_1$ )-*b*-PS ( $r = 1$ ) sample obtained during the heating and cooling processes. Upon heating high-order reflections develop gradually (Figure 3a), and at 160 °C the SAXS pattern shows multiple reflections with a  $q$  ratio of 1:2:3:4, which is characteristic of a highly ordered lamellar structure. The intensities of the high-order reflections decrease after cooling (Figure 3b).

We also compared the phase behaviors of the DLBCPs with different salt concentrations at 160 °C, which is far above their  $T_g$ 's. All the SAXS profiles of LiCF<sub>3</sub>SO<sub>3</sub>-doped PEG( $G_m$ )-*b*-PS at  $r = 0$  to 1 measured at a constant temperature of 160 °C are displayed in Figure 4. These profiles show lithium salt



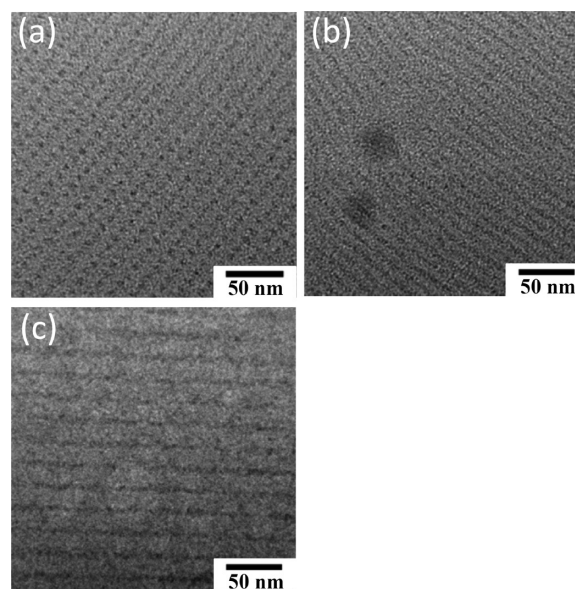
**Figure 3.** SAXS profiles of the PEG( $G_1$ )-*b*-PS DLBCP with doped LiCF<sub>3</sub>SO<sub>3</sub> ( $r = 1$ ) during the heating (a) and cooling (b) processes. The curves at different temperatures are shifted in the vertical direction for clarity.

concentration dependence of phase behavior. For PEG( $G_1$ )-*b*-PS, where  $r = 0$ , no scattering peaks are seen in the SAXS profile, indicating that the neat polymer is disordered. Incorporation of small amounts of LiCF<sub>3</sub>SO<sub>3</sub> into disordered PEG( $G_1$ )-*b*-PS, as shown in Figure 4a for  $r = 0.02$ , the SAXS pattern is essentially identical to the undoped DLBCP, indicating that the system remains disordered. When  $r = 0.05$ , a strong scattering peak is developed, indicating that an increase in salt concentration leads to microphase separation. However, higher-order reflections are not detected. Increasing molar ratio of [Li] to [EO] to  $r = 0.1$ , two more peaks appear in addition to a sharp scattering peak located at  $q^* = 0.426 \text{ nm}^{-1}$  in the SAXS pattern, with a  $q$  ratio of 1:3<sup>1/2</sup>:2, which is characteristic of a two-dimensional HEX structure. From the primary reflection, the  $d_{100}$  value is determined to be 14.7 nm (corresponding to an intercolumn distance of 17.0 nm). As the dendritic block has a weight fraction of 0.14, it forms the core (with PEG in the center) in the HEX structure and is encapsulated by the PS block. As  $r$  increases further to 1, the SAXS profile indicates a lamellar morphology with the first-order peak  $q$  value of  $0.267 \text{ nm}^{-1}$ . The primary peak moves toward lower  $q$  as the amount of LiCF<sub>3</sub>SO<sub>3</sub> increases, as shown in Figure 4a. TEM experiments were conducted to confirm the morphologies. Figure 5a,b shows cylinder morphologies viewed parallel and perpendicular to the cylinder axis. The column-to-column distance is estimated to be  $\sim 16 \text{ nm}$ , consistent with the SAXS data. Alternating layers are seen when  $r = 1$  for PEG( $G_1$ )-*b*-PS in Figure 5c.



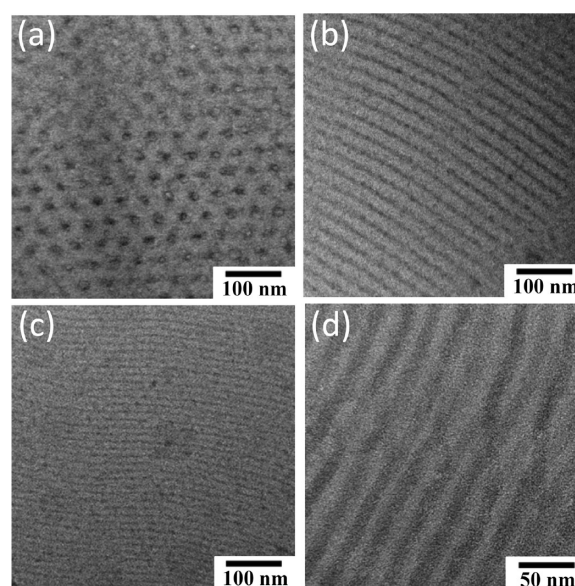
**Figure 4.** SAXS profiles of the blends of DLBCPs PEG( $G_1$ )-*b*-PS (a), PEG( $G_2$ )-*b*-PS (b), and PEG( $G_3$ )-*b*-PS (c) with different contents of  $\text{LiCF}_3\text{SO}_3$ . The curves at different salt contents are shifted in the vertical direction for clarity.

Figure 4b shows the SAXS profiles of PEG( $G_2$ )-*b*-PS doped with lithium salt of similar contents. The results are similar to those of the  $G_1$  DLBCP. Again, the neat polymer is disordered. When  $r = 0.02$ , the scattering peak developed gradually. When  $r = 0.05$ , the SAXS profile exhibits three distinctive peaks located at  $q^*$ ,  $1.73q^*$ , and  $2q^*$ , indicative of a HEX morphology. From the primary peak, the intercolumn distance is calculated to be 26.8 nm. When  $r = 0.1$  and 1, the SAXS patterns display multiple reflections with  $q$  ratios of 1:2:3 and 1:2:3:4, respectively, consistent with lamellar structures. TEM experiments were also conducted to further confirm the microstructures and micrographs at different lithium concentrations were obtained. The results are in agreement with the SAXS data. When  $r = 0.05$ , the TEM micrograph shows hexagonal patterns of dark PEG domains surrounded by bright PS



**Figure 5.** TEM micrographs of lithium-doped PEG( $G_1$ )-*b*-PS when  $r = 0.1$  (a, b) and 1 (c).

domains (Figure 6a). When  $r = 0.1$  and 1, alternating PEG and PS layers (Figure 6c,d) are observed.



**Figure 6.** TEM micrographs of lithium-doped PEG( $G_2$ )-*b*-PS when  $r = 0.05$  (a, b), 0.1 (c), and 1 (d).

Figure 4c shows the SAXS profiles of PEG( $G_3$ )-*b*-PS doped with lithium salt. However, the SAXS patterns are different from those of the  $G_1$  and  $G_2$  polymers. The profile of the neat polymer shows a primary reflection, indicating a microphase-separated system. Increasing  $r$  to 0.02 and up to 1, the  $G_3$  DLBCP blends demonstrate lamellar structures with a shift in the primary peak position, revealing that the lamellar spacing increases with increasing salt concentration. The phenomenon was confirmed by TEM results shown in Figure 7.

The effect on the microstructures induced by the addition of  $\text{LiCF}_3\text{SO}_3$  to the DLBCPs can be mainly attributed to changes in the interaction parameter  $\chi$  that influences phase behavior. The results show that adding  $\text{LiCF}_3\text{SO}_3$  increases the degree of

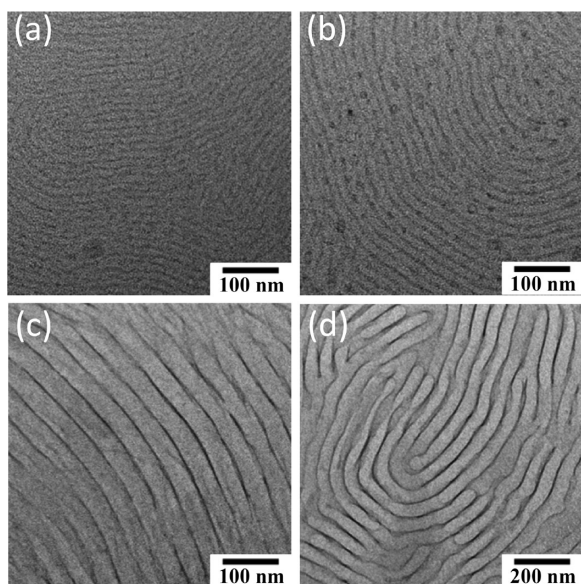


**Figure 7.** TEM micrographs of lithium-doped PEG( $G_3$ )-*b*-PS when  $r = 0.02$  (a),  $0.05$  (b),  $0.1$  (c), and  $1$  (d).

segregation between the dendritic and linear blocks, driving the material toward the strong-segregation regime.<sup>30,31</sup>

**Effect of Dendron Generation on Polymer Morphology.** Besides the volume fraction, the dendron generation is a crucial parameter that influences phase behavior, elucidating the role of shape-induced interface curvature in the microstructure formation. To simplify the discussion, we assume that  $f$  is constant when the salt concentration is the same for DLBCPs of different generations with an equal weight fraction.

Figure 8 shows the phase diagram using the SAXS results of lithium salt-doped DLBCPs with  $[Li]/[EO]$  in the range 0–1.

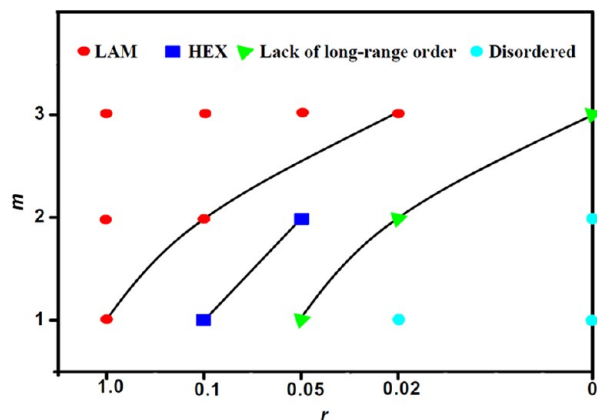


**Figure 8.** Phase diagram of DLBCPs depending on dendron generation and salt concentration.

The  $y$ -axis is the generation of the dendritic block. The phase diagram is composed of three parts. The first part at lower right is the disordered morphology for neat polymers and blends at low lithium salt contents. When the lithium salt concentration increases, microphase separation begins to occur. And the critical salt content to induce microphase separation decreases with increasing dendron generation. When  $r = 0.02$ , the three blends of different generations show different self-assembly behaviors. The blends of  $G_1$  and  $G_2$  DLBCPs are disordered, while the  $G_3$  DLBCP blend exhibits a lamellar structure. When

$r = 0.05$ , the  $G_1$  DLBCP blend is still disordered but shows a scattering peak at  $0.456 \text{ nm}^{-1}$  and the  $G_2$  DLBCP blend shows a HEX structure, while the  $G_3$  DLBCP blend retains a lamellar structure. As the salt content increases further to  $r = 0.1$ , the  $G_1$  DLBCP blend forms a HEX structure, while the  $G_2$  blend transforms into a lamellar structure. Meanwhile, the  $G_3$  DLBCP blend is still lamellar, with an increased layer spacing. When  $r = 1$ , the blends of all  $G_m$  DLBCPs form lamellar structures. The above discussion indicates that the blends of  $G_1$  and  $G_2$  DLBCPs both undergo phase transitions from HEX morphologies to lamellar structures with increasing content of  $\text{LiCF}_3\text{SO}_3$ , while the  $G_3$  DLBCP blends only form lamellar structures.

The morphological differences between samples with different dendron generations at equal dendron weight fractions are strongly attributed to the difference in the degree of chain branching. As discussed by Fredrickson, the phase boundaries are significantly shifted toward lower dendron volume fraction as the number of generation or the functionality of the branch points increases.<sup>32</sup> Therefore, for the DLBCPs investigated in this work, the blends of  $G_1$  and  $G_2$  DLBCPs both undergo transformations from HEX to LAM, while the  $G_3$  DLBCP blend retains LAM for all salt concentrations. The results agree well with the theory. We speculate that further reducing the dendron volume fraction of the  $G_3$  DLBCP may cause the system to form a HEX morphology.

**Conductivity of PEG( $G_3$ )-*b*-PS ( $r = 1$ ).** We measured the conductivity of lithium-doped PEG( $G_3$ )-*b*-PS with  $r = 1$ . Normal-to-plane conductivity data were obtained at three different temperatures. The impedance spectra at different temperatures are shown in Figure 9. The thickness of the film is  $300 \text{ nm}$ , and the area is  $1.8 \times 10^{-4} \text{ m}^2$ . The conductivity value is calculated to be  $9.1 \times 10^{-7} \text{ S/cm}$  at  $30 \text{ }^\circ\text{C}$  and  $1.0 \times 10^{-5} \text{ S/cm}$  at  $75 \text{ }^\circ\text{C}$ . As shown in Figure 9b, the ionic conductivity increases gradually upon heating. This behavior is consistent with higher ionic and segmental mobilities at higher temperatures. Ionic conductivities for polymers at other lithium concentrations were not measured because of poor film-forming ability and insufficient amount of samples for the measurements. However, through subtle structural modifications in the linear block of the DLBCPs, polymer electrolyte with good mechanical and film forming properties may be developed.

## CONCLUSIONS

In summary, we have prepared a series of dendritic–linear block copolymers with an equal dendron volume fraction. The dendritic block is composed of a semirigid Percec-type dendron, and the periphery of the dendron is ionophilic PEG. The linear block was synthesized by NMRP. Their molecular characteristics were determined by NMR, GPC, and MALDI-TOF MS as the connection point of the two blocks can be hydrolyzed. The thermal properties and phase behaviors of  $\text{LiCF}_3\text{SO}_3$ -doped PEG( $G_m$ )-*b*-PS DLBCPs as a function of lithium salt concentration and dendron generation were studied. Doping the salt drives microphase separation toward the strong-segregation limit because of the increase in the effective Flory–Huggins interaction parameter  $\chi$  between the two blocks. Studies on salt concentration dependence of phase behavior show disordered, HEX, and LAM morphologies for blends of  $G_1$  and  $G_2$  DLBCPs while  $G_3$  DLBCP blends display lamellar structures throughout the whole salt concentration range studied. The difference may originate from the different

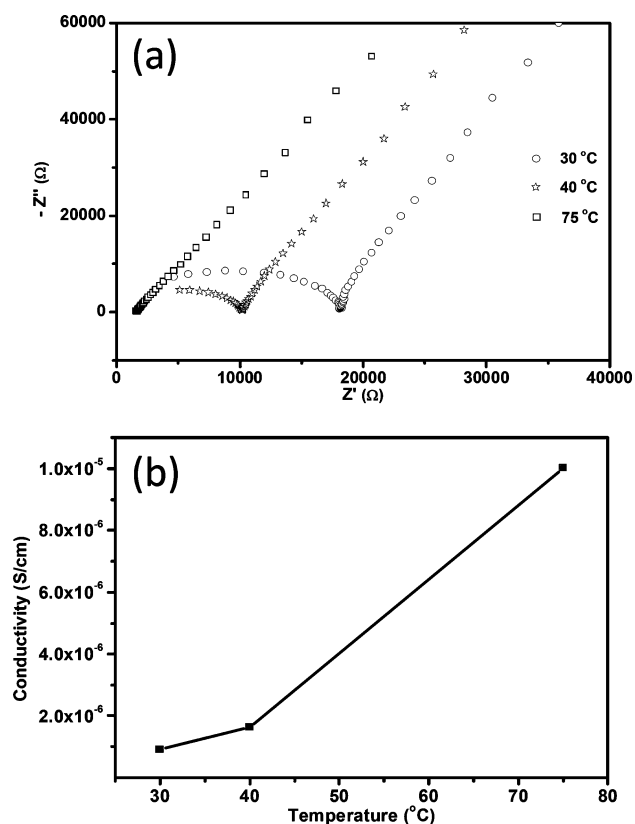


**Figure 9.** Impedance spectra (a) and temperature dependence of ionic conductivity (b) of lithium-doped PEG( $G_3$ )-*b*-PS ( $r = 1$ ) at different temperatures.

degree of chain branching, which leads to different interface curvature. The study on the effect of morphology on the ionic conductivity of the dendritic-linear block copolymers with ionophilic PEG is still in progress.

## ■ ASSOCIATED CONTENT

### 📄 Supporting Information

Data of  $^1\text{H}$  NMR of the dendron intermediates of different generations and the dendritic macroinitiators,  $^{13}\text{C}$  NMR data of  $G_2$ -COOH and  $G_3$ -COOH, GPC profile and MALDI-TOF result of the dendritic macroinitiators, GPC profiles of DLBCPs before and after hydrolysis, DSC thermograms of  $G_1$  and  $G_2$  DLBCPs without and with doped  $\text{LiCF}_3\text{SO}_3$  of different concentrations. This material is available free of charge via the Internet at <http://pubs.acs.org>.

## ■ AUTHOR INFORMATION

### Corresponding Author

\*E-mail: [fanxh@pku.edu.cn](mailto:fanxh@pku.edu.cn) (X.F.); [zshen@pku.edu.cn](mailto:zshen@pku.edu.cn) (Z.S.).

### Notes

The authors declare no competing financial interest.

## ■ ACKNOWLEDGMENTS

This research was supported by the National Natural Science Foundation of China (Grants 21134001 and 20974002).

## ■ REFERENCES

(1) Bates, F. S.; Fredrickson, G. H. *Annu. Rev. Phys. Chem.* **1990**, *41*, 525–557.

(2) Epps, T. H.; Bailey, T. S.; Waletzko, R.; Bates, F. S. *Macromolecules* **2003**, *36*, 2873–2881.

(3) Warren, S. C.; Messina, L. C.; Slaughter, L. S.; Kamperman, M.; Zhou, Q.; Gruner, S. M.; DiSalvo, F. J.; Wiesner, U. *Science* **2008**, *320*, 1748–1752.

(4) Rosen, B. M.; Wilson, C. J.; Wilson, D. A.; Peterca, M.; Imam, M. R.; Percec, V. *Chem. Rev.* **2009**, *109*, 6275–6540.

(5) Gitsov, I.; Wooley, K. L.; Hawker, C. J.; Ivanova, P. T.; Fréchet, J. M. J. *Macromolecules* **1993**, *26*, 5621–5627.

(6) Mackay, M. E.; Hong, Y.; Jeong, M.; Tande, B. M.; Wagner, N. J.; Hong, S.; Gido, S. P.; Vestberg, R.; Hawker, C. J. *Macromolecules* **2002**, *35*, 8391–8399.

(7) Yu, D.; Vladimirov, N.; Fréchet, J. M. J. *Macromolecules* **1999**, *32*, 5186–5192.

(8) Pyun, J.; Tang, C.; Kowalewski, T.; Fréchet, J. M. J.; Hawker, C. J. *Macromolecules* **2005**, *38*, 2674–2685.

(9) Magbitang, T.; Lee, V. Y.; Cha, J. N.; Wang, H.-L.; Chung, W. R.; Miller, R. D.; Dubois, G.; Volksen, W.; Kim, H.-C.; Hedrick, J. L. *Angew. Chem., Int. Ed.* **2005**, *44*, 7574–7580.

(10) Gillies, E. R.; Jonsson, T. B.; Fréchet, J. M. J. *J. Am. Chem. Soc.* **2004**, *126*, 11936–11943.

(11) Iyer, J.; Fleming, K.; Hammond, P. T. *Macromolecules* **1998**, *31*, 8757–8765.

(12) del Barrio, J. S.; Oriol, L.; Sánchez, C.; Serrano, J. L.; Di Cicco, A. I.; Keller, P.; Li, M.-H. *J. Am. Chem. Soc.* **2010**, *132*, 3762–3769.

(13) Wurm, F.; Frey, H. *Prog. Polym. Sci.* **2011**, *36*, 1–52.

(14) Wu, J.; Tang, H.; Wu, P. *Soft Matter* **2011**, *7*, 1185–1191.

(15) Wu, J.; Tang, H.; Wu, P. *Soft Matter* **2011**, *7*, 4166–4169.

(16) Grason, G. M.; DiDonna, B. A.; Kamien, R. D. *Phys. Rev. Lett.* **2003**, *91*, 058304.

(17) Cho, B.-K.; Jain, A.; Gruner, S. M.; Wiesner, U. *Chem. Commun.* **2005**, 2143–2145.

(18) Chung, Y.-W.; Lee, J.-K.; Zin, W.-C.; Cho, B.-K. *J. Am. Chem. Soc.* **2008**, *130*, 7139–7147.

(19) Lee, E.; Lee, B.-I.; Kim, S.-H.; Lee, J.-K.; Zin, W.-C.; Cho, B.-K. *Macromolecules* **2009**, *42*, 4134–4140.

(20) Kim, H.-Y.; Song, J.; Kim, S.-H.; Lee, E.; Lee, J.-K.; Zin, W.-C.; Cho, B.-K. *Chem.—Eur. J.* **2009**, *15*, 8683–8686.

(21) Cho, B.-K.; Kim, S.-H.; Lee, E. *J. Polym. Sci., Part A: Polym. Chem.* **2010**, *48*, 2372–2376.

(22) Malkoch, M.; Schleicher, K.; Drockenmuller, E.; Hawker, C. J.; Russell, T. P.; Wu, P.; Fokin, V. V. *Macromolecules* **2005**, *38*, 3663–3678.

(23) Rajakumar, P.; Srinivasan, K. *Tetrahedron* **2004**, *60*, 10285–10291.

(24) Stoll, R. S.; Hecht, S. *Org. Lett.* **2009**, *11*, 4790–4793.

(25) Bothe, M.; Schmidt-Naake, G. *Macromol. Rapid Commun.* **2003**, *24*, 609–613.

(26) Wu, C.-Y.; Brik, A.; Wang, S.-K.; Chen, Y.-H.; Wong, C.-H. *ChemBioChem* **2005**, *6*, 2176–2180.

(27) Hua, C.; Peng, S.-M.; Dong, C.-M. *Macromolecules* **2008**, *41*, 6686–6695.

(28) Kose, M. M.; Onbulak, S.; Yilmaz, I. I.; Sanyal, A. *Macromolecules* **2011**, *44*, 2707–2714.

(29) Liang, W.-J.; Chen, Y.-P.; Wu, C.-P.; Kuo, P.-L. *J. Phys. Chem. B* **2005**, *109*, 24311–24318.

(30) Young, W.-S.; Epps, T. H. *Macromolecules* **2009**, *42*, 2672–2678.

(31) Wanakule, N. S.; Virgili, J. M.; Teran, A. A.; Wang, Z.-G.; Balsara, N. P. *Macromolecules* **2010**, *43*, 8282–8289.

(32) Frischknecht, A.; Fredrickson, G. H. *Macromolecules* **1999**, *32*, 6831–6836.